

Framework Fe Ions in Fe-ZSM-5 Zeolite Studied by UV Resonance Raman Spectroscopy and Density Functional Theory Calculations

Keju Sun,^{†,‡} Fengtao Fan,^{†,‡} Haian Xia,^{†,‡} Zhaochi Feng,[†] Wei-Xue Li,^{*,†} and Can Li^{*,†}

State Key Laboratory of Catalysis, Dalian Institute of Chemical Physics, Chinese Academy of Sciences, 457 Zhongshan Road, Dalian 116023, China, and Graduate University of Chinese Academy of Sciences, Beijing 100049, China

Received: April 5, 2008; Revised Manuscript Received: July 3, 2008

The transition metal containing zeolites show high selectivity and activity in many catalytic reactions under mild conditions; however, detailed characterization of transition metal site ions and the nature of the active sites remain elusive. Here, we present a study of the framework Fe ions in Fe-ZSM-5 zeolite via interplay between resonance Raman spectroscopy excited by 244 and 532 nm laser lines and density functional theory (DFT) calculations. Raman bands at 1165, 1115, 1005, and 516 cm^{-1} from the framework iron ions in the framework of Fe-ZSM-5 were observed. On the basis of the DFT calculations, the bands at 1165, 1115, and 516 cm^{-1} were attributed to $\nu_0(\text{A}_1)$, $\nu_1(\text{A}_1)$, and $\nu_2(\text{A}_1)$ modes with totally symmetric vibration of FeO_4 tetrahedron in Fe-ZSM-5, originating from resonant enhanced Raman scattering, while the band at 1005 cm^{-1} for $\nu_6(\text{T}_2)$ was identified as a nontotally symmetric vibration of the FeO_4 tetrahedron from normal Raman scattering. The present work indicates that the resonance Raman bands at 500 and 1100 cm^{-1} can be used as the spectral characteristics of the transition metal ions substituted in the framework of zeolites.

1. Introduction

The transition metal (TM) containing zeolites such as Fe-ZSM-5,^{1–3} FeAPO-5,⁴ and Ti-Silicalite-1⁵ have received wide attention due to their high activity and selectivity in many catalytic reactions, particularly in selective oxidation under mild conditions. Despite great effort devoted to the characterization of TM ions containing zeolites, the characterization of the structures of TM ions in zeolites is still difficult because of the low concentrations and complexity of structures. Furthermore, the TM ions in zeolite may adopt different forms, e.g. in Fe-ZSM-5, isolated iron sites at ion-exchange positions, binuclear iron sites, oligonuclear iron oxide clusters, and framework iron ions (replacing Si or Al in a T-site), etc.⁶ Resonance Raman spectroscopy is unique spectroscopy to differentiate different species from a complex molecular system such as TM ions containing zeolites by varying the wavelength of excited laser lines.⁷ On the other hand, density functional theory (DFT) calculations can provide not only the energetic/kinetics of possible structures and chemical reactions, but also the vibrational information in terms of the vibrational frequency and modes, which can be used to compare with available experimental data.^{8–10} Thus, the structures of the TM ions in zeolites could be identified by the interplay between the Raman spectroscopy and DFT calculations. However, the explicit calculation of resonance Raman spectra of zeolites has remained a challenge due to the complexity of zeolite and computational demands.¹¹

The assignment of the resonance Raman spectrum of framework TM in zeolite is not very clearly studied, which prevents further study about the synthesis mechanism of zeolite by UV

resonance Raman spectroscopy. To shed new light on the framework TM ions in zeolites, we report here a cooperative study on the iron ions in Fe-ZSM-5 by combining UV resonance Raman, visible Raman spectroscopy, and density functional theory calculations. Various Raman spectra have been measured by using different excited laser lines, and analyzed in detail by DFT calculations. The nature of the individual Raman bands has been identified and supplemented by symmetry analysis based on DFT. A characteristic of spectra for the TM ions in the framework of zeolites was proposed.

2. Experimental and Computational Methods

2.1. Experimental Section. The Fe-ZSM-5 sample was synthesized with template-free methods to reduce the influence of organic impurity on the spectra. The sample was synthesized by adding ZSM-5 seeds (1% of the mass of the silica) to the crystallization gel with a molar composition of $12\text{Na}_2\text{O}:1(\text{Al}_2\text{O}_3/\text{Fe}_2\text{O}_3):38\text{SiO}_2:1400\text{H}_2\text{O}$ and the crystallization period for 60 h was followed. The detailed procedure was described elsewhere.¹² In gel, the Si/Al ratio is 25.3 and the Si/Fe ratio is 76.0. With ICP (Inductively Coupled Plasma) analysis on the sample after crystallization, the Si/Al ratio is 28.6 and the Si/Fe ratio is 66.7. The structure of samples synthesized showed typical MFI structure, as verified by X-ray diffraction (not shown). The UV–vis diffuse reflectance spectrum and UV Raman spectrum were recorded at room temperature and ambient atmosphere. UV–vis diffuse reflectance spectra were recorded on a JASCO V-550 UV–vis spectrophotometer. UV Raman spectra were measured with a Jobin-Yvon T64000 triple-stage spectrograph with spectral resolution of 2 cm^{-1} . The laser line at 325 nm of a He–Cd laser was used as an exciting source with an output of 25 mW. The power of the laser at the sample was about 1.0 mW. The 244 nm line from a Coherent Innova 300 Fred laser with power around 1.0 mW on sample was used. Visible Raman spectra were recorded on a Jobin-Yvon U1000 scanning double monochromator with the spectral resolution of 4 cm^{-1} . The line

* To whom correspondence should be addressed. Tel: 86-411-84379996. Fax: 86-411-84694447. E-mail: wxli@dicp.ac.cn (W.X.L.). Homepage: <http://www.tc.dicp.ac.cn>, Tel: 86-411-84379070. Fax: 86-411-84694447. E-mail: canli@dicp.ac.cn (C.L.). Homepage: <http://www.canli.dicp.ac.cn>.

[†] Chinese Academy of Sciences.

[‡] Graduate University of Chinese Academy of Sciences.

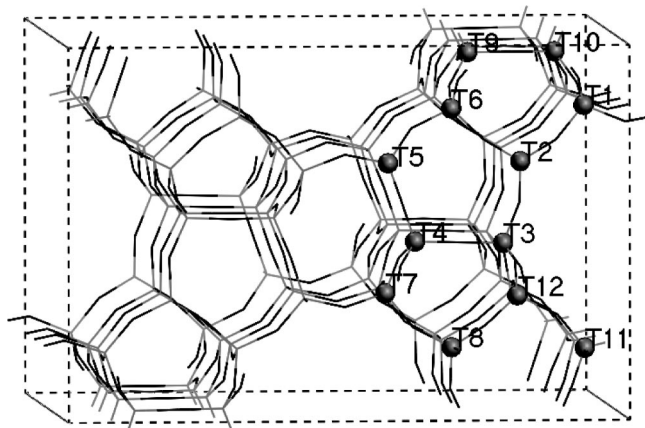


Figure 1. Schematic structure for Fe-ZSM-5. T $_n$ ($n = 1-12$) represents 12 possible sites substituted isomorphously by iron ion.

at 532 nm from a DPSS 532 Model 200 532 nm single-frequency laser was used as the excitation source. The accumulation time for the spectrum is 50, 300, and 600 s for laser lines 532, 325, and 244 nm, respectively.

2.2. Computational Methods. Our applied DFT is based on periodic methods. Periodic methods place the region of interest in periodic boundary conditions and usually employ a full quantum mechanical treatment for the whole system, thus overcoming a number of the shortcomings of the molecular cluster approach. These approaches have been widely used in studies of metal and semiconductor, as well as metal/metal oxide and halide interfaces where the delocalized electron states are of importance. Periodic DFT calculations have been performed with use of the Vienna Ab Initio Simulation Package (VASP).¹³ The total energy was calculated by solving the Kohn–Sham equations, using the exchange–correlation functional proposed by Perdew and Zunger,¹⁴ corrected for nonlocality in the generalized gradient approximation with PW91 functional.¹⁵ VASP uses plane waves to expand wave functions, PAW potentials,¹⁶ allowing a significant reduction of the number of plane waves. For the present calculations, a cutoff of 400 eV and a Brillouin-zone sampling restricted to the Γ -point have been used. All the ions in the super cell are relaxed until the residual force on each ion is less than 0.05 eV \AA^{-1} .

When a quadrivalent Si cation in the zeolite framework was replaced by a trivalent iron cation, an extra monovalent cation was added to maintain the charge neutrality of the system. In our studies, H^+ was selected as a compensative cation. A super cell of MFI structure with dimensions of 20.0 $\text{\AA} \times 19.9 \text{\AA} \times 13.4 \text{\AA}$, which includes overall 289 ions, was used to simulate the Fe-ZSM-5 zeolite containing a single framework iron ion. The structure was shown schematically in Figure 1, where there are 12 possible tetrahedral sites in MFI (initial structure parameters come from Atlas of Zeolite Structures¹⁷) structure for Fe substitution, which were considered in the present work. The setup of the large supercell is used because it enables us to compare reliably the relative stability of various Fe substitution sites.

Since the unit cell volume depends strongly on the content of the heteroatoms in zeolite,¹⁸ optimization of unit cell lattice constants and all internal atoms was performed simultaneously to minimize the total energy and residual stress to zero. To calculate the frequency, the finite differences method was employed. In these calculations, the unit cell was fixed at the optimized lattice constants, and the iron ion and the 33 surrounding ions around were allowed to be displaced by 0.04

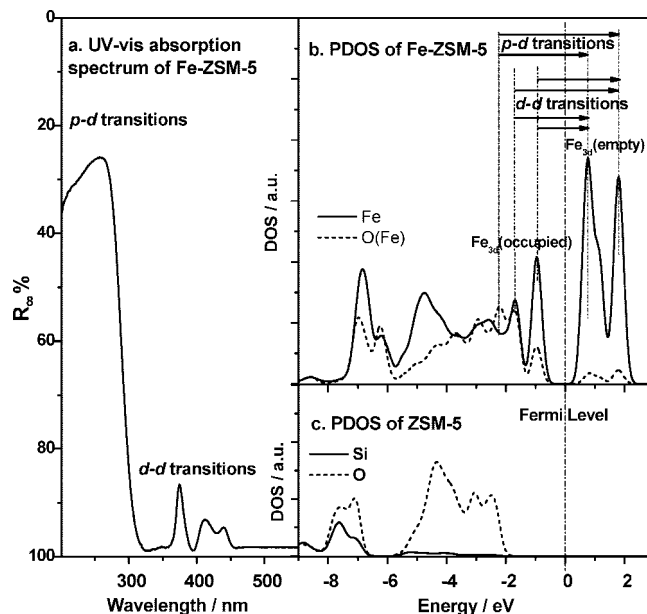


Figure 2. (a) UV–vis diffuse reflectance spectrum of Fe-ZSM-5. (b) Calculated projected density of states (PDOS) of the Fe and coordinated O ions in Fe-ZSM-5 and (c) for Si and coordinated O ions in ZSM-5.

\AA in the three directions of the Cartesian coordinate. We note that it is important to include a sufficient number of neighbor ions around Fe to get complete vibration spectra for physical comparison with available experimental spectra. The convergence test with respect to the number of displaced ions around Fe was found to be significant and the small number of displaced ions will result in a considerable error bar. More important, some vibration modes involving more than the nearest neighbor atoms, as seen in the present work, cannot be obtained unless a sufficiently large number of displaced ions around Fe have been considered. To compare with experimental results, all the computed frequencies were multiplied by a factor of 1.05.¹⁹

3. Results

3.1. Electronic Transitions and Raman Spectra of Fe-ZSM-5. We describe below the experimental measurement first. In Figure 2a, the UV–vis diffuse reflectance spectrum of Fe-ZSM-5 was shown, where five distinct absorption bands centered at 250 nm with significant intensity and 376, 413, 438, and 480 nm with weak intensity can be seen. The strong absorption at 250 nm comes mainly from p–d charge transfer transition between the framework oxygen anion and the iron cation in Fe-zeolite, while four bands at 376, 413, 438, and 480 nm come from the d–d transitions of Fe^{3+} in tetrahedral coordination environment.^{20–22} As a rule of thumb, these bands are believed to be the direct evidence of the existence of framework iron ions in zeolite.^{21,23,24} A dedicated preparation method has been employed to minimize possible agglomeration of Fe and formation of extra framework Fe. The Fe-ZSM-5 sample was synthesized without templates therefore the calcinations were avoided and the Fe species was fixed in the framework of the zeolite. The iron species were mainly located in the framework, which was corroborated further by the absence of typical absorption bands from the extra framework iron species, which typically fall in range from 300 to 600 nm within the UV–vis reflectance spectrum (Figure 2a). When laser lines 325 and 532 nm were used as excited lines (Figure 4), there are no pronounced new peaks present. All these lead consistently to

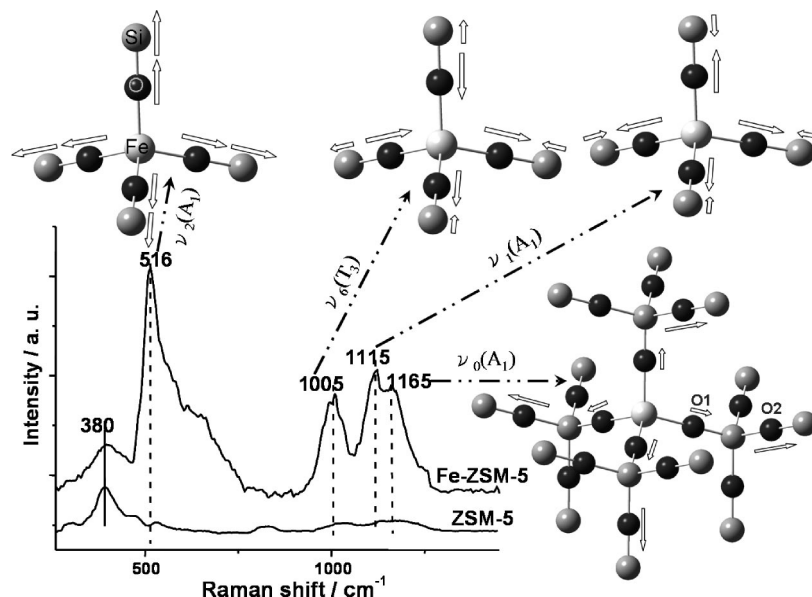


Figure 3. Raman spectra of Fe-ZSM-5 and ZSM-5 excited by 244 nm laser line and schematic ball-stick models for four possible vibrational modes, $\nu_0(A_1)$, $\nu_1(A_1)$, $\nu_2(A_1)$, and $\nu_6(T_2)$, of 4-fold framework iron cation in zeolites.

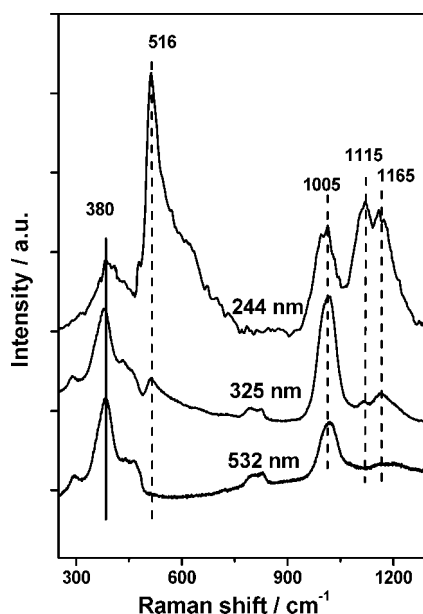


Figure 4. Raman spectra of Fe-ZSM-5 with excitation lines at 244, 325, and 532 nm, respectively.

the conclusion that only the bands involved in the framework Fe species would be enhanced in the resonance Raman spectra of Fe-ZSM-5, and the contribution from extra framework heterogeneous Fe species if there is any should be negligible.

The above analysis was substantiated by projected density of state (PDOS) of the framework Fe tetrahedron in Fe-ZSM-5 from DFT calculation. Since there are overall 12 possible tetrahedral substituted sites for Fe in the ZSM-5 structure, their structures and stabilities were studied first. In the present work, a significant large supercell with overall 289 atoms allowed us to study all possible Fe substitution sites. With use of this setup, their relative stability can be compared straightforward. As discussed above, only framework Fe was considered. The calculated total energies for optimized Fe-ZSM-5 with framework Fe substituted at different tetrahedral sites were listed in Table 1. It can be found that the energetically most favorable site for Fe substitution is T4, and T11 is meta stable and 4 kJ

TABLE 1: Calculated Total Energies (in kJ mol⁻¹) for Optimized Fe-ZSM-5 with Framework Iron Substituted at Different Tetrahedral Sites

substituted sites	total energy	substituted sites	total energy
T1	-220183.8	T7	-220187.3
T2	-220180.8	T8	-220187.0
T3	-220182.9	T9	-220179.1
T4	-220193.5	T10	-220185.0
T5	-220180.0	T11	-220189.5
T6	-220181.6	T12	-220187.2

mol⁻¹ higher. The next favorable sites are T7, T12, and T8 (2 kJ mol⁻¹ higher than T11). The remaining structures are energetically significantly higher and the concentration for Fe substitution in these sites should be considerable lower. It should be noted that the thermal energy under ambient conditions is around 2 kJ mol⁻¹.²⁵ Hence, under thermodynamic equilibrium conditions, the population of T4 substitution should dominate, but the population at T11, T7, T12, and T8 sites may still be significant. To simplify the analysis, only the structure for Fe substitution at the T4 site was considered below. However, the conclusions obtained were found to be less dependent on this. Our test calculations showed that the calculated density of states and frequencies, as well as their vibrational modes of Fe-ZSM-5, were rather independent of specific substitutional sites, which is understandable because similar local tetrahedral symmetry was applied on them.

Figure 2b showed the calculated PDOS of the Fe cation and coordinated O ion nearby in Fe-ZSM-5. For reference, the PDOS of the Si and coordinated O ions in ZSM-5 zeolite was calculated and plotted in Figure 2c. As shown in Figure 2b, due to the presence of iron, iron orbitals hybridize with those of oxygen in the wide range of energy windows from -7 to -1 eV with respect to the Fermi level. In contrast to this, the hybridization between Si and O in ZSM-5 was limited to a narrow energy window, which was followed by a huge gap (the bottom of the conduction band was not shown here) as expected from the insulator nature of ZSM-5, while for Fe-ZSM-5, the gap decreases dramatically to 1.7 eV due to the presence of Fe d orbitals, which lowers the bottom of the conduction band. We note that the band gap derived nowadays from DFT is often

underestimated due to approximation of exchange–correlation interaction employed in DFT.

Because about half of the d electronic states were occupied, d electrons of Fe³⁺ could be excited from the occupied states (below Fermi level) to the unoccupied d-states when the sample was irradiated with proper excitation lines. Correspondingly, d–d transitions were observed in the UV–vis absorption spectrum (Figure 2a). Within the same energy window (below Fermi level), there is a significant population from p orbitals of O²⁻ available, and p–d transitions may occur as indicated in Figure 2a,b. The calculated PDOS of Fe-ZSM-5 therefore suggests that both of the p–d transitions and d–d transitions could appear for Fe-ZSM-5 with framework Fe in tetrahedral coordination, which was absent for ZSM-5 otherwise. The calculated results agree well with the measured UV–vis diffuse reflectance spectrum.

Figure 3 showed the Raman spectrum of Fe-ZSM-5 zeolite and ZSM-5 zeolite for reference excited by the 244 nm laser. Since the 244 nm laser line falls in the energy range for p–d transitions of Fe-ZSM-5, the Raman spectrum of Fe-ZSM-5 was attributed to a resonance-enhanced Raman spectrum. Five strong Raman bands at 380, 516, 1005, 1115, and 1165 cm⁻¹ were observed in the spectrum of Fe-ZSM-5 zeolite. Among of them, the band at 380 cm⁻¹ was a typical band of the five-membered building unit of ZSM-5 zeolite.^{26,27} Compared to the Raman spectrum of ZSM-5 zeolite, the Fe-ZSM-5 zeolite spectrum presents additional bands at 516, 1005, 1115, and 1165 cm⁻¹. These bands should be related to the framework tetrahedral Fe ions since there was no characteristic spectra of extraframework iron ions observed from the UV–vis diffuse reflectance spectrum. To clarify the nature of bands measured, the vibrational modes and frequencies of framework tetrahedral Fe were studied further by DFT calculations.

3.2. Spectral Analysis. It is well-known that for Raman spectroscopy, only the vibrational modes, which involve the electronic transitions, could be enhanced considerably. In a system like Fe-ZSM-5, the 244 nm excitation line falls energetically in the region of p–d transition between p orbitals of O²⁻ and d orbitals of Fe³⁺. Correspondingly, mainly the vibrational modes, which involve the vibration of FeO₄ tetrahedron, could be enhanced. Therefore, the vibration modes involving the strong vibration of FeO₄ tetrahedron were considered.

According to the resonance Raman scattering theory,^{28,29} there are three primary mechanisms for enhancement, so-called A, B, and C terms. The C-term would dominate only enhancement for resonance excitation within forbidden electronic transitions. In the system of Fe-ZSM-5, the electronic transition is strongly allowed, since a strong absorption band at 250 nm was observed in the UV absorption spectrum and assigned to charge transfer from O²⁻p to Fe³⁺d. The C-term contribution can therefore be excluded. In general, B-term enhancement would dominate in transitions where significant oscillator strength derives from Herzberg–Teller coupling to adjacent strongly allowed transitions. In this situation, both symmetric and nonsymmetric vibration modes can be enhanced. The A-term would dominate the enhancement in strongly allowed transitions. In most cases, A-term resonance related mainly by totally symmetric vibration modes is enhanced. However, when A-term scattering involves a change of symmetry in the resonant excited state or excited state Jahn–Teller coupling, nontotally symmetric modes may also occur.^{30–32} Therefore, although there are situations where nontotally symmetric vibrations will be enhanced more than totally symmetric vibrations, the totally symmetric vibrations

TABLE 2: Calculated and Experimental Vibration Frequencies (cm⁻¹) of Fe-ZSM-5 and ZSM-5

	theory		exptl (Fe-ZSM-5)
	(Fe-ZSM-5)	(ZSM-5)	
$\nu_0(A_1)$	1147	1258	1165
$\nu_1(A_1)$	1130	1230	1115
$\nu_6(T_2)$	1050	1153	1005
	1031	1145	1005
	1009	1132	1005
$\nu_2(A_1)$	514	528	516

usually would be more extensive than those of nontotally symmetric vibrations in strongly allowed transitions.

Guided by these principles, a set of modes $\nu_6(T_2)$, $\nu_0(A_1)$, $\nu_1(A_1)$, and $\nu_2(A_1)$, with considerable displacements of the normal coordinates for the FeO₄ unit have, been screened from calculated numerous vibrational frequencies and modes, which were listed in Table 2 and plotted in Figure 3, respectively. Among of them, $\nu_6(T_2)$ was a nontotally symmetric vibrational mode, while it was totally symmetric for the remaining $\nu_0(A_1)$, $\nu_1(A_1)$, and $\nu_2(A_1)$ modes. These different modes are discussed further below.

The calculated frequency for the $\nu_0(A_1)$ mode (see Figure 3) was 1147 cm⁻¹. In this mode, Fe–O stretching was driven by the stretching vibration of neighbor Si–O–Si. Our calculations showed that the relative displacement of the oxygen ion (O2 in Figure 3) in Si–O–Si was larger than that of the oxygen ion (O1) in Fe–O–Si. According to the calculated vibrational frequency, the observed band at 1165 cm⁻¹ in the UV resonance Raman spectrum of Fe-ZSM-5 was attributed to the $\nu_0(A_1)$ mode.

For the $\nu_1(A_1)$ mode, the calculated frequency was 1130 cm⁻¹. In the UV resonance Raman spectrum of Fe-ZSM-5, a band was observed at 1115 cm⁻¹ with significant intensity. The agreement of vibration frequency between experiment and theory led us to assign the measured band at 1115 cm⁻¹ to the $\nu_1(A_1)$ mode. In our previous work,³³ TS-1 zeolite has been studied in detail by UV resonance Raman spectroscopy and a band at 1124 cm⁻¹ was observed and attributed to the $\nu_1(A_1)$ mode too.¹¹

The calculated $\nu_2(A_1)$ mode was similar to the $\nu_1(A_1)$ mode. The difference was that the vibration of the silicon ion of the $\nu_1(A_1)$ mode was out of phase with respect to the vibration of the oxygen ion, but in phase for the $\nu_2(A_1)$ mode (see Figure 3 for details). The synchronization of silicon and oxygen ions results in considerably lower frequency of $\nu_2(A_1)$ than $\nu_1(A_1)$ partially due to the increase of the effective mass for the previous one. Indeed, the calculated frequency of the $\nu_2(A_1)$ mode was 514 cm⁻¹ in contrast to 1130 cm⁻¹ for $\nu_1(A_1)$. In the UV resonance Raman spectra, the measured band at 516 cm⁻¹ in Fe-ZSM-5 with pronounced high intensity was assigned to the $\nu_2(A_1)$ mode, accordingly.

The $\nu_6(T_2)$ mode was the only nontotally symmetric stretching vibrational mode of FeO₄, as seen clearly from Figure 3. For the isolated tetrahedron complex, this mode would have triplex degeneracy (T₂). The symmetry was broken, however, in the present due to the lower symmetry of the surroundings. The $\nu_6(T_2)$ band was split into three bands with calculated values at 1050, 1031, and 1009 cm⁻¹ (slightly lower than that of the $\nu_1(A_1)$ mode, 1130 cm⁻¹). In the UV resonance Raman spectra of Fe-ZSM-5, a band at 1005 cm⁻¹ was observed and attributed to the $\nu_6(T_2)$ mode accordingly. It was possible that three vibrations have different response in terms of Raman scattering, thus three split bands exist but only one was observed.

4. Discussions

The assignment of $\nu_6(T_2)$ with the nontotally symmetric vibration of FeO_4 tetrahedrons to the UV resonance Raman band 1005 cm^{-1} with significant intensity was apparently counter intuitive. According to the theory of resonance Raman scattering discussed earlier, nontotally symmetric modes will not be involved in the resonance Raman scattering unless the electronic excitation induces pronounced structural distortion of molecules or B-term resonance scattering.^{30–32} Due to the constraint of the extended zeolite framework, the excitation induced structural deformation of FeO_4 within the framework of ZSM-5 zeolite would be rather limited. B-term enhancement dominates in transitions where significant oscillator strength derives from Herzberg–Teller coupling to adjacent strongly allowed transitions, so-called vibronically electronic coupling. Though we cannot exclude the possibility of the $\nu_6(T_2)$ driven by the resonance scattering, the possibility is expected to be low.

It is likely that though the band at 1005 cm^{-1} was observed in the UV Raman spectrum excited by the 244 nm laser line, in which resonance-enhanced Raman bands dominated, it may come from the normal Raman scattering with intensity comparable to resonance Raman scattering. To test this assumption, Raman spectra of Fe-ZSM-5 were measured using 325 and 532 nm excited lines, and plotted in Figure 4. Since the energy corresponding to 325 or 532 nm is well below the energy required for the p–d transition of Fe-ZSM-5, possible resonance enhanced Raman scattering can be excluded. Nevertheless, a strong band at about 1005 cm^{-1} was observed in the Raman spectra of Fe-ZSM-5 with 532 nm excitation, and the bands at 516, 1115, and 1165 cm^{-1} from resonance-enhanced Raman scattering spectra were fully absent. This clearly showed that the band at 1005 cm^{-1} did come from nonresonant Raman scattering.

Above calculations showed that all identified bands at 516, 1005, 1115, and 1165 cm^{-1} were related to framework tetrahedral Fe ions, and could therefore be used as a proof of existence of framework Fe ions with local tetrahedral symmetry. As seen clearly from the above discussions, the bands at 1005 and 1165 cm^{-1} involved the ions beyond FeO_4 tetrahedron, and it is expected that their intensity would be sensitive to the specific location of the substituted Fe. In other words, the bands would be sensitive to the surrounding structures of the framework Fe, so they may provide some detailed information, such as the zeolite crystallization and the compensative ions. In contrast, the presence of the bands at 516 and 1115 cm^{-1} could be used as reliable evidence for the existence of the framework Fe ions with tetrahedral coordination in ZSM-5 zeolites.

Because the substituted transition metal ions in the framework of various zeolites share similar local symmetry with tetrahedral coordination, they should show similar resonance Raman spectra as the Fe-ZSM-5 zeolite described here. In the past, the bands at 530 and 1125 cm^{-1} in the resonance Raman spectrum of TS-1⁷ and at 510 and 1090 cm^{-1} in resonance Raman spectrum of Fe-SBA-15³⁴ were observed and readily attributed to the framework Ti ions and Fe ions with tetrahedral coordination, respectively. Therefore, the bands at about 500 and 1100 cm^{-1} observed in resonance Raman spectra could be regarded as the characteristic bands for the existence of the substituted transition metal ions in the framework of a wide range of zeolites. In principle, for ZSM-5, the characteristic normal coordinates identified here should exist, as is verified by our calculations with frequency 528 and 1230 cm^{-1} (Table 2). However, because of the absence of the TM ion the possible resonance Raman scatter is prohibited. For normal Raman scattering, on the other

hand, the poor signal-to-noise ratio limits the direct observation of these spectra.

5. Conclusions

In summary, the framework Fe in Fe-ZSM-5 was studied in detail by interplay between UV resonance Raman spectroscopy experiments and density functional theory calculations. Raman bands at 516, 1005, 1115, and 1165 cm^{-1} excited by the 244 nm laser line were detected. The bands at 516, 1115, and 1165 cm^{-1} from resonant Raman scattering are attributed to the totally symmetric vibrations $\nu_2(A_1)$, $\nu_1(A_1)$, and $\nu_0(A_1)$ of FeO_4 tetrahedron in the framework of Fe-ZSM-5. In contrast, the Raman band at 1005 cm^{-1} was attributed to the nontotally symmetric vibration $\nu_6(T_2)$, which originated from normal Raman scattering. It is proposed that the bands at about 500 and 1100 cm^{-1} observed in resonance Raman spectra of transition metal substituted zeolites could be the characteristic features for the presence of the transition metal ions with tetrahedral coordination in the framework sites of zeolites.

Acknowledgment. The authors are grateful to the Program for Strategic Scientific Alliances between China and The Netherlands (PSA), the Royal Netherlands Academy of Arts and Sciences (KNAW) (Grant No. 04-PSA-M-01), and the National Basic Research Program of China (Grant No. 2004CB720607) for financial support. W.X.L. thanks NSFC (Grant No. 20621063) for financial support.

References and Notes

- (1) Panov, G. I.; Kharitonov, A. S.; Sobolev, V. I. *Appl. Catal. A* **1993**, *98*, 1.
- (2) Panov, G. I.; Uriarte, A. K.; Rodkin, M. A.; Sobolev, V. I. *Catal. Today* **1998**, *41*, 365.
- (3) Pirutko, L. V.; Chernyavsky, V. S.; Uriarte, A. K.; Panov, G. I. *Appl. Catal. A* **2002**, *227*, 143.
- (4) Raja, R.; Sankar, G.; Thomas, J. M. *J. Am. Chem. Soc.* **1999**, *121*, 11926.
- (5) Clerici, M. G.; Bellussi, G.; Romano, U. *J. Catal.* **1991**, *129*, 159.
- (6) Pirngruber, G. D.; Roy, P. K.; Prins, R. *Phys. Chem. Chem. Phys.* **2006**, *8*, 3939.
- (7) Li, C. *J. Catal.* **2003**, *216*, 203.
- (8) Nachtigallová, D.; Bludský, O.; Otero Areán, C.; Bulánek, R.; Nachtigall, P. *Phys. Chem. Chem. Phys.* **2006**, *8*, 4849.
- (9) Garrone, E.; Bulánek, R.; Frollich, K.; Otero Areán, C.; Rodríguez Delgado, M.; Palomino, G. T.; Nachtigallová, D.; Nachtigall, P. *J. Phys. Chem. B* **2006**, *110*, 22542.
- (10) Benco, L.; Bucko, T.; Hafner, J.; Toulhoat, H. *J. Phys. Chem. B* **2004**, *108*, 13656.
- (11) Ricchiardi, G.; Damin, A.; Bordiga, S.; Lamberti, C.; Spano, G.; Rivetti, F.; Zecchina, A. *J. Am. Chem. Soc.* **2001**, *123*, 11409.
- (12) Fan, F. T.; Sun, K. J.; Feng, Z. C.; Xia, H. A.; Han, B.; Lian, Y. X.; Ying, P. L.; Li, C. A spectroscopic understanding of the synthesis mechanism of Fe-ZSM-5. *J. Am. Chem. Soc.*, submitted for publication, 2008.
- (13) (a) Kresse, G.; Hafner, J. *Phys. Rev. B* **1993**, *48*, 13115. (b) Kresse, G.; Hafner, J. *Phys. Rev. B* **1994**, *49*, 14251. (c) Kresse, G.; Furthmüller, J. *Comput. Mater. Sci.* **1996**, *6*, 15. (d) Kresse, G.; Furthmüller, J. *Phys. Rev. B* **1996**, *54*, 11169.
- (14) Perdew, J. P.; Zunger, A. *Phys. Rev. B* **1981**, *23*, 5048.
- (15) Perdew, J. P.; Burke, K.; Wang, Y. *Phys. Rev. B* **1996**, *54*, 16533.
- (16) (a) Blöchl, P. E. *Phys. Rev. B* **1994**, *50*, 17953. (b) Kresse, G.; Joubert, J. *Phys. Rev. B* **1999**, *59*, 1758.
- (17) Data from Atlas of zeolite structures. <http://www.ch.ic.ac.uk/vchemlib/course/zeolite/atlas.html>.
- (18) Lamberti, C.; Bordiga, S.; Zecchina, A.; Carati, A.; Fitch, A. N.; Artioli, G.; Petrini, G.; Salvalaggio, M.; Marra, G. L. *J. Catal.* **1999**, *183*, 222.
- (19) Travert, A.; Dujardin, C.; Maugé, F.; Veilly, E.; Cristol, S.; Paul, J. F.; Payen, E. *J. Phys. Chem. B* **2006**, *110*, 1261.
- (20) Goldfarb, D.; Bernardo, M.; Strohmaier, K. G.; Vaughan, D. E. W.; Thomann, H. *J. Am. Chem. Soc.* **1994**, *116*, 6344.
- (21) Lin, D. H.; Coudurier, G.; Vedrine, J. *Zeolites: Facts, Figures, Future*; Jacobs, P. A., van Santen, R. A., Eds.; Elsevier: Amsterdam, The Netherlands, 1989; p 1431.

- (22) Patarin, J.; Tuilier, M.; Durr, J.; Kessler, H. *Zeolites* **1992**, *12*, 70.
- (23) Bordiga, S.; Buzzoni, R.; Geobaldo, F.; Lamberti, C.; Giamello, E.; Zecchina, A.; Leofanti, G.; Petrini, G.; Tozzola, G.; Vlaic, G. *J. Catal.* **1996**, *158*, 486.
- (24) Marturano, P.; Drozdová, L.; Pirngruber, G. D.; Kogelbauer, A.; Prins, R. *Phys. Chem. Chem. Phys.* **2001**, *3*, 5585.
- (25) Gale, J. D. *Solid State Sci.* **2006**, *8*, 234.
- (26) (a) Dutta, P. K.; Puri, M. *J. Phys. Chem.* **1987**, *91*, 4329. (b) Dutta, P. K.; Rao, K. M.; Park, J. Y. *J. Phys. Chem.* **1991**, *95*, 6654.
- (27) Astorino, E.; Peri, J. B.; Willey, R. J.; Busca, G. *J. Catal.* **1995**, *157*, 482.
- (28) Stair, P. C. *Adv. Catal.* **2007**, *51*, 75.
- (29) Asher, S. A. *Annu. Rev. Phys. Chem.* **1988**, *39*, 537.
- (30) Long, D. A. *The Raman Effect: A Unified Treatment of the Theory of Raman Scattering by Molecules* John Wiley & Sons Ltd.: Chichester, England, 2002; p 221.
- (31) Nishimura, Y.; Hirakawa, A. Y.; Tsuboi, M. *Advances in Infrared and Raman Spectroscopy*; Clark, R. J. H., Hester, R. E., Eds.; Heyden & Son: London, UK, 1978.
- (32) Carey, P. R. *Biochemical Application of Raman and Resonance Raman Spectroscopies*; Academic Press: New York, 1982.
- (33) Li, C.; Xiong, G.; Xin, Q.; Liu, J.; Ying, P.; Feng, Z.; Li, J.; Yang, W.; Wang, Y.; Wang, G.; Liu, X.; Lin, M.; Wang, X.; Min, E. *Angew. Chem., Int. Ed.* **1999**, *38*, 2220.
- (34) Li, Y.; Feng, Z. C.; Xin, H. C.; Fan, F. T.; Zhang, J.; Magusin, P. C. M. M.; Hensen, E. J. M.; van Santen, R. A.; Yang, Q. H.; Li, C. *J. Phys. Chem. B* **2006**, *110*, 26114.

JP802955S